Available online at www.sciencedirect.com
ScienceDirect
Journal of the European Ceramic Society 29 (2009) 1995–2001
www.elsevier.com/locate/jeurceramsoc

Microstructure and grain size dependence of ferroelectric properties of $BaTiO_3$ thin films on $LaNiO_3$ buffered Si

Liang Qiao, Xiaofang Bi *

Key Laboratory of Aerospace Materials and Performance (Ministry of education), School of Materials Science and Engineering, Beijing University of Aeronautics and Astronautics, Xue yuan Road, 37# Hai dian District, Beijing 100083, China

Received 12 August 2008; received in revised form 18 November 2008; accepted 24 November 2008
Available online 22 January 2009

Abstract

$BaTiO_3$ films were prepared by radio frequency sputtering on the $LaNiO_3$/Si substrates and then annealed at different temperatures. The films exhibit a highly (1 0 0)-oriented structure and their grain size range from 14 to 55 nm after annealing. Polarization-reversal characteristics for different $BaTiO_3$ films were measured. The results show that while obvious ferroelectricity is obtained for films with grain size larger than 22 nm, a weak ferroelectricity is still observed in $BaTiO_3$ film of 14 nm grains, indicating that if a critical grain size exists for ferroelectricity it is less than 14 nm for polycrystalline $BaTiO_3$ on $LaNiO_3$/Si. The suppression of macroscopic ferroelectricity for $BaTiO_3$ with finest grain size and the grain size dependence of remnant polarization and coercive field are also discussed in detail.
© 2008 Elsevier Ltd. All rights reserved.

Keywords: $BaTiO_3$ and titanates; Films; Grain size; Ferroelectric properties; Perovskites

1. Introduction

Perovskite $BaTiO_3$ (BTO) ceramics have been extensively studied due not only to their excellent electrical properties and other associated effects but also to their lead-free characteristics.[1] In recent years BTO thin films have received much attention with the development of microelectronics and integrated optics technologies.[2] With downsizing one dimension to nano-scale or submicron, however, the thin films exhibit more or less deviations in structure and properties as compared to their bulk or single crystal counterparts.[3,4] In addition, for device applications, conducting electrodes are required to explore the ferroelectric properties of the thin films. Meanwhile, many efforts have been made to form a BTO thin film on Si substrates buffered with a conductive layer. Metal films such as Pt or Pt/Ti are most often used as bottom electrodes due to their excellent conductive characterizations. However, compared to the metallic electrodes, the perovskite-related metallic oxide electrodes, such as $La_{0.5}Sr_{0.5}CoO_3$, $SrRuO_3$ and $LaNiO_3$ have been found to lead to a great improvement of the fatigue and aging of ferroelectric memories,[5,6] which is unavoidable with the metallic electrodes. Among those oxide electrodes, the $LaNiO_3$ (LNO) thin film has been developed as a promising metal oxide electrode, due to its simple chemical composition, preferential growth with (1 0 0) orientation and its little lattice mismatch with ferroelectric materials.

On the other hand, it is known that both microstructure and properties of ferroelectric films are dependent greatly on buffer layers and fabrication processes.[7–10] The extrinsic parameters are also assumed to be responsible for variations in microstructure dependence of ferroelectricty, and might be the reason for a broad dispersion in some data such as critical size below which ferroelectricity is eradicated. For example, in the last two decades, there had been a variety of different experimental critical thickness for epitaxial ferroelectric thin films.[11–16] However, recent theoretical and experimental studies have implied that there is no intrinsic thickness limit for ferroelectricity in thin films with thickness down to even several unit cells.[17,18] While for ferroelectric polycrystalline films, nano-particles, or nanoceramics, there is still no unambiguous conclusion that if there exists a critical grain size responsible for the disappearance of the macroscopic ferroelectricity. Meanwhile, the experimental studies on the grain size dependence of ferroelectricity for the

* Corresponding author. Tel.: +86 10 82339231.
E-mail addresses: liang@mse.buaa.edu.cn (L. Qiao), bixf@buaa.edu.cn (X. Bi).

0955-2219/$ – see front matter © 2008 Elsevier Ltd. All rights reserved.
doi:10.1016/j.jeurceramsoc.2008.11.017

BTO thin films onto the LNO buffered Si substrates are still rare in the literature. In this work, BTO films with same thicknesses were annealed at different temperatures, transmission electron microscopy (TEM) has been used to obtain the morphology and grain size of the BTO films. The ferroelectric properties for different films were measured and their grain size dependence were also investigated and discussed.

2. Experimental

Ferroelectric BTO thin films and conductive LNO buffer layers were fabricated in a multi-targets radio frequency (rf) sputtering system on (1 0 0) Si substrates. The LNO target was prepared by the conventional ceramic powder processing with lanthanum oxide and nickel(III) oxide as starting materials. The LNO buffer layers of 200 nm were deposited directly on (1 0 0) silicon substrate at 600 °C. In order to avoid the oxygen loss for the oxides films, mixed atmosphere of argon and oxygen was introduced (2 Pa:2 Pa for LNO films and 3 Pa:1 Pa for BTO films) during the deposition process. The ferroelectric BTO thin films of 200 nm were subsequently deposited onto the LNO buffer layers at room temperature. The as-deposited films were then annealed in an open-air atmosphere with different temperatures ranging from 400 to 800 °C for 2 h in order to obtain different grain size.

The structure and crystal orientation of the films were characterized by θ–2θ scans of Cu Kα X-ray diffraction (XRD, D/max2200PC, Rigaku). Surface morphology of the films was observed by atomic force microscopy (AFM, SPI 3800N, SEIKO). Interface structures were observed by field-emission scanning electron microscopy (FESEM, HTACHI S4500). Film thicknesses were measured by DektakII profiler and calibrated by FESEM images. The grain size of the BTO films were estimated from transmission electron microscopy (TEM, JEOL 2100F) images and the film orientation was also characterized by the corresponding electron diffraction pattern. The electrical properties were determined by a metal–ferroelectric–metal (MFM) structure. Ferroelectric properties of the films were investigated using standard Sawyer-Tower circuit by TF analyzer 2000 measurement system (aixACCT, Germany).

3. Results and discussion

Fig. 1 presents the XRD pattern of the LNO buffer layer deposited on Si substrate, along with its surface morphology (inset of the figure) observed by AFM. It can be seen that the as-deposited LNO film exhibits a crystalline phase with a high (1 0 0) orientation. The AFM morphology shows that the film is dense and uniform, with the average grain size of 20–30 nm. The resistivity of the films measured by four-probe testing system is as low as 8.4×10^{-4} Ω cm at room temperature, indicating that the LNO films can be used as an electrode. BTO films were then deposited on the LNO buffered Si at room temperature. Fig. 2(a) shows the XRD patterns of the BTO films annealed at several different temperatures. When the annealing temperature is 400 °C, only (1 0 0) and (2 0 0) peaks for LNO can be observed and no any other peaks related with BTO can be identified, indicating that the BTO films remain an amorphous structure at the temperature. When the annealing temperature is increased to 500 °C, a broadened (2 0 0) peak ascribed to the BTO start to appear. With further increasing the annealing temperature,

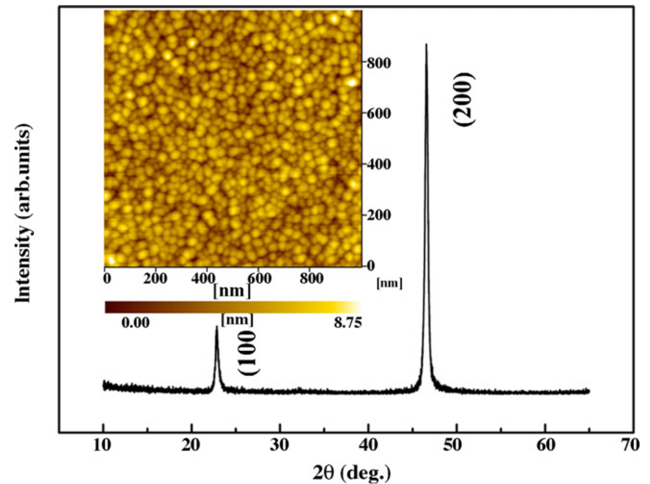

Fig. 1. XRD pattern of the LNO thin film deposited on Si substrate. The inset is an AFM surface morphology.

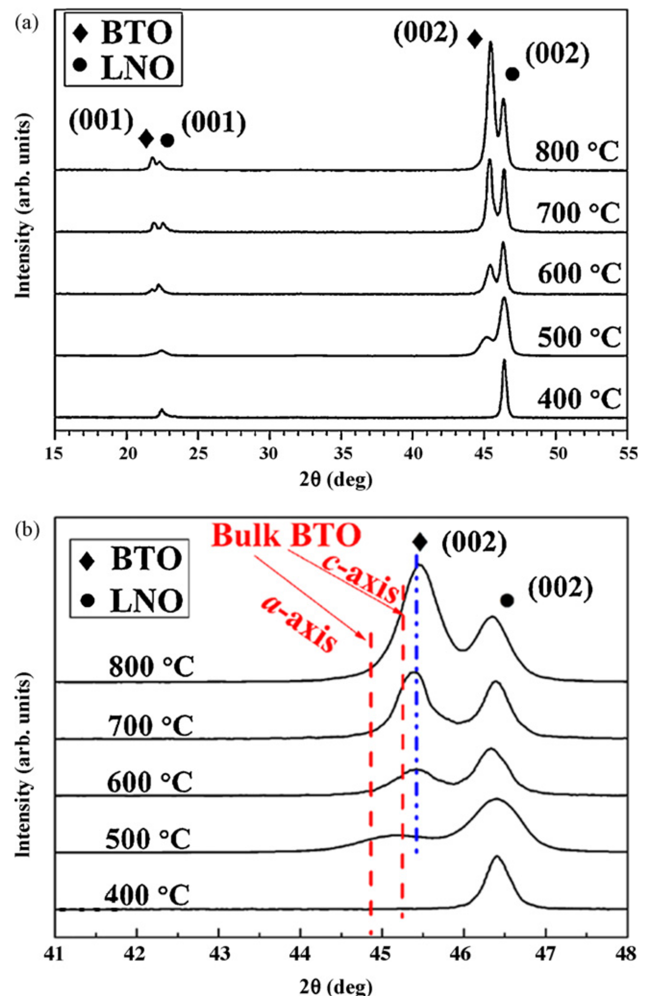

Fig. 2. (a) XRD patterns of the BTO films annealed at different temperatures ranging from 400 to 800 °C and (b) magnified view of XRD patterns in (a).

the peaks become much sharper and are gradually intensified. From the results, it can be obtained that the BTO films start to crystallize at 500 °C from the amorphous phase and grow into a (1 0 0) preferred orientation on the LNO (1 0 0) buffered Si substrates as the annealing temperatures increase. As we had pointed out,[19,20] the (1 0 0) preferred orientation for the BTO films is attributed to the (1 0 0)-oriented LNO seed layer due to the little lattice mismatch (3.75%) between (0 0 1) [1 0 0] LNO and (0 0 1) [1 0 0] BTO lattice. From the magnified view of XRD patterns in Fig. 2(b), the lattice constants as well as strain states for both BTO and LNO layers can also be extracted. As can be seen, the (0 0 2) peaks for all the LNO layers are positioned at the same diffraction angel, indicating the LNO films possess same lattice constant, which is calculated to be 3.91 Å. Compared with that of bulk LNO (3.84 Å), the larger value reveals that LNO films are under tensile strain state, due to large difference in thermal expansion coefficients (TECs) between LNO underlayer ($8.2 \times 10^{-6}\,K^{-1}$) and Si substrate ($1.4 \times 10^{-6}\,K^{-1}$). On the other hand, compared with the 2θ peak position of bulk BTO (red dashed lines), these BTO (0 0 2) 2θ diffraction peaks are shifted to higher angles, indicating a decrease in the out-of-plane lattice constants and an increase in the in-plane lattice constants in the BTO films. Since the LNO layer is very thin compared with Si, so the shift is suggested to be the result of the thermal strain induced during the cooling process caused by the difference of TECs between BTO layer ($10.4 \times 10^{-6}\,K^{-1}$) and Si substrate.[21] This corresponds well with the experimental result that BTO tends to form an in-plane tensile strain state when incorporated with Si substrate.[21,22] Nevertheless, as the (0 0 2) peaks for all the BTO layers are almost at the same position (blue dashed lines), so the BTO layers are also under same strain state in spite of different annealing temperature.

Microstructures for the annealed films were characterized by plan-view TEM observations, as shown in Fig. 3(a)–(d). It is clearly seen that the films annealed at temperatures ≥500 °C are crystallized and featured as uniform and cracks-free. The grain size is increased with increasing the annealing temperatures, changing from 14 to 55 nm in diameter, as summarized in Table 1. It is noted that the BTO films in this work exhibit much smaller grain sizes as compared to other reported BTO films.[23,24] The difference is considered to be the result of the influence of microstructure of the LNO buffer layer. It is known that grain size for a newly formed crystal is dependent on the nucleation rate and the growth rate, respectively. In this work, the

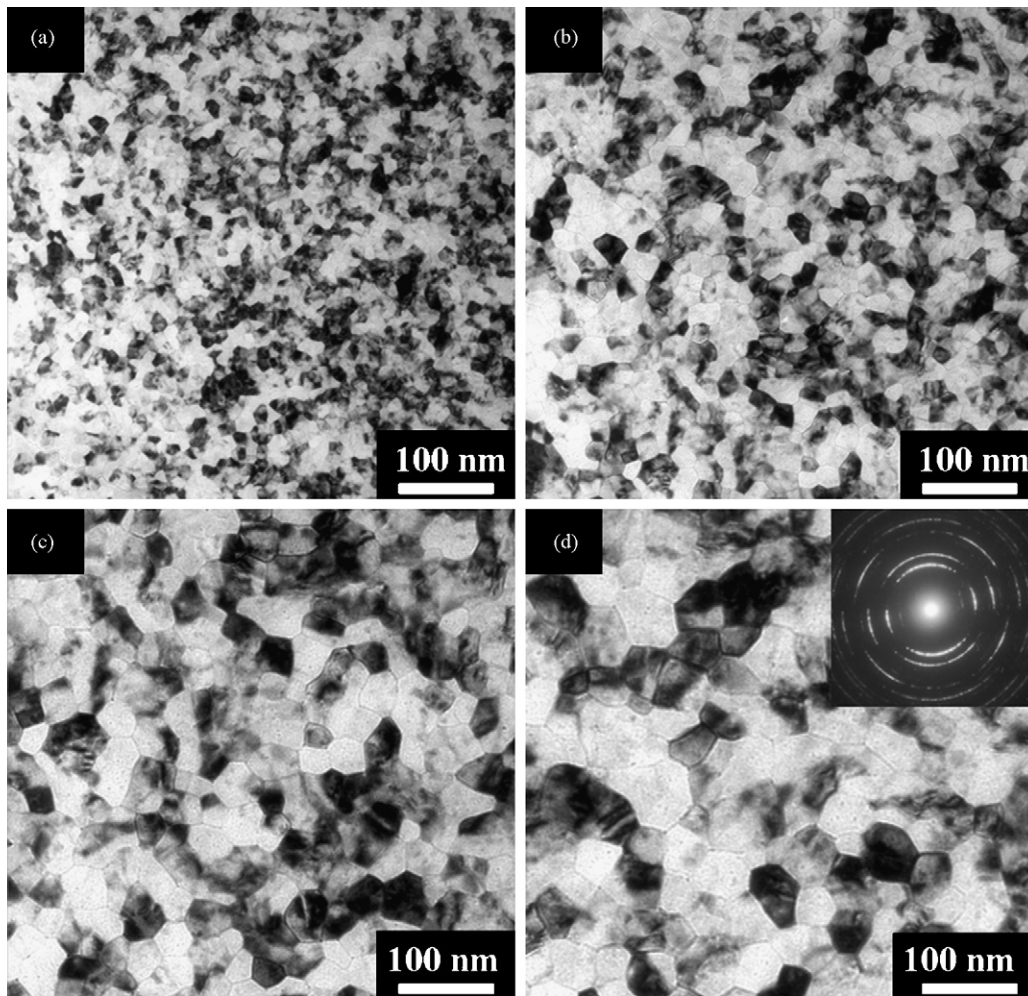

Fig. 3. Plan-view TEM images of the BTO film annealed at different temperatures: (a) 500 °C, (b) 600 °C, (c) 700 °C and (d) 800 °C. The inset is the electron diffraction arc for the 800 °C-annealed film.

Table 1
Effect of annealing temperatures on the grain size for the $BaTiO_3$ films.

Annealing temperature (°C)	Average grain size (nm)
500	14
600	20–25
700	30–40
800	50–60

LNO buffer layer with very fine grain size of 20–30 nm was used as seed layers for the ferroelectric BTO films. The grain boundaries in the LNO buffer layers will act as nucleation sites for the crystallization of the BTO films during the annealing processes. The smaller grain size of the LNO film leads to more nucleation sites for the crystallization of BTO films and, as a result, the BTO films grow into a microstructure characterized by fine and uniform grains. In order to investigate the preferential orientation of the BTO films with nano-scaled grains, an electron diffraction pattern was observed with a tilt angle of 20° between the electron beam direction and the film normal (Si [0 0 1]) direction. The inset of Fig. 3(d) shows the electron diffraction pattern for the 800 °C-annealed film. The pattern is characterized by arc shapes. According to Tang et al.'s explanation[25,26] the appearance of the arc shape pattern demonstrates the existence of a preferred [0 0 1] fiber-texture, which also agrees with the previous XRD results (in Fig. 2) that the BTO films annealed at 800 °C have a strong (0 0 1) orientation. The arc-shaped pattern has been also observed in other films after annealing at temperatures ≥500 °C. Therefore, the sharper and intensified peak with higher annealing temperatures observed in the XRD profiles is ascribed mainly to the grain growth in the BTO films.

The surface morphologies of BTO films annealed at different temperatures had also been analyzed by AFM observations, as shown in Fig. 4(a)–(c). The 400 °C-annealed BTO film exhibits an amorphous structure without the formation of any distinct grains on the surface and increasing annealing temperature will increase the BTO grain size, which agrees well with the XRD and TEM results. With increasing the annealing temperature, the

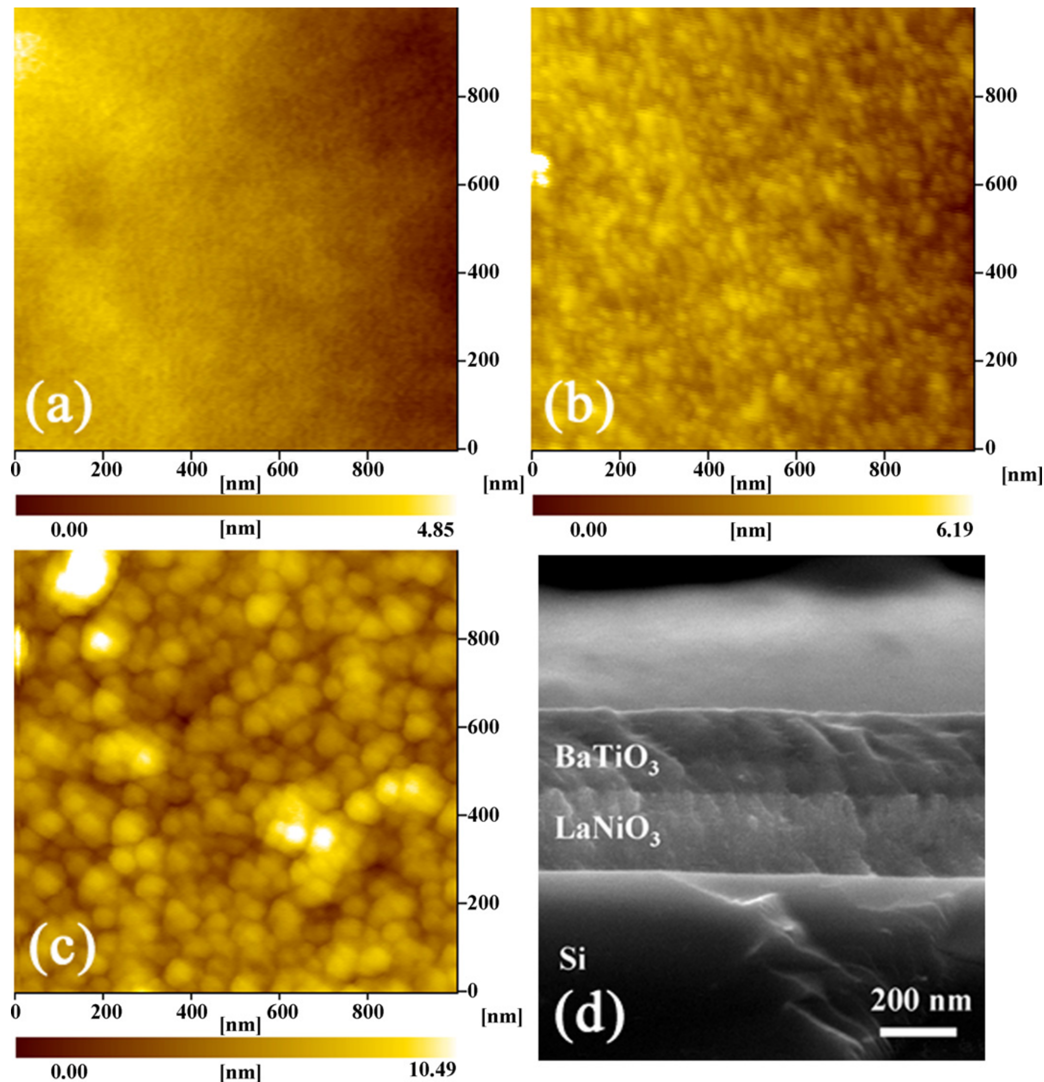

Fig. 4. AFM surface morphologies for BTO films annealed at (a) 400 °C, (b) 500 °C and (c) 800 °C. (d) The interface structure of BTO/LNO bi-layer annealed at 800 °C.

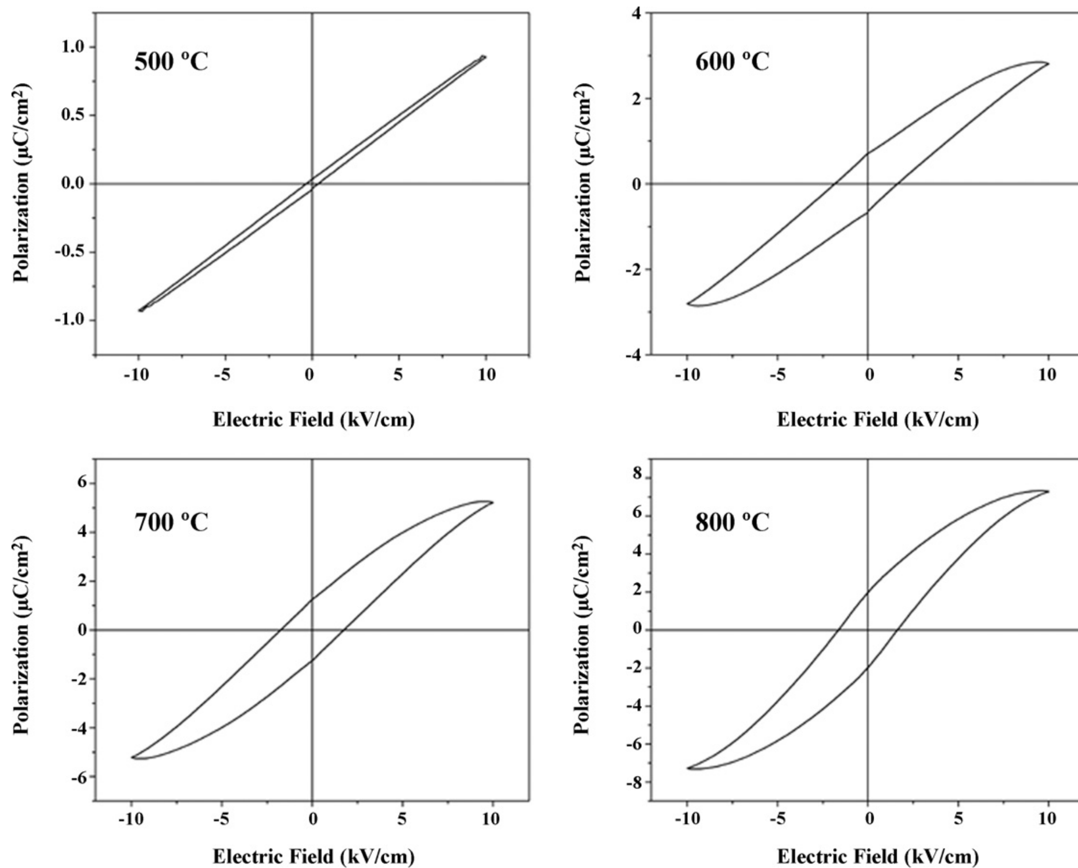

Fig. 5. Hysteresis loops of the BTO films after annealing at different temperatures.

root mean square (RMS) value of BTO surface roughness is also increased, from RMS = 4.85 nm at 400 °C to RMS = 10.49 nm at 800 °C. Fig. 4(d) shows the interface structure of BTO/LNO bilayer annealed at 800 °C. It seems that the high temperature annealing does not result in severe interdiffusion between the two layers as their interface is still obvious and sharp.

Room temperature ferroelectric hysteresis loops of the BTO films annealed at different temperatures are described in Fig. 5(a)–(d) . As can be seen, for BTO films annealed at 600 °C and above, obvious hysteretic shape of polarization vs. electric field (*P*–*E*) curves are obtained. With increasing the annealing temperature, the *P*–*E* hysteresis loop starts to become much more erect and saturated, showing a typical ferroelectric characterization. The obtained remnant polarization (P_r) for 800 °C-annealed BTO is 2.0 μC/cm^2, similar to the values of other polycrystalline BTO films, e.g. 2.0 μC/cm^2 on Pt/Ti/TiO_x/Si by Thomas et al.[27] and 1.0 μC/cm^2 on Pt/SiO_2/Si by Huang et al.[3] However, compared with the value for BTO single crystal (24 μC/cm^2) or other epitaxial BTO films,[28,29] the P_r is still much lower, probably due to fine grain size and the formation of in-plane tensile strain state on the Si substrate, as had been obtained by the XRD analysis. On the other hand, for BTO film with the finest grain size of 14 nm (annealed at 500 °C), it still exhibits some hysteresis characteristics with P_r ~0.08 μC/cm^2, although it is not obvious and shows almost linear dependence of $P(E)$. This corresponds well with the recently reported experimental results that the ferroelectricity does exist in nanocrystalline BTO ceramics with ultra fine grain size of 30 nm,[1] 22 nm,[30] and even 8 nm.[31] However, the significantly reduced P_r is indicative of a strong suppression of macroscopic ferroelectric character in the 14 nm BTO film, which may arise from either the frozen domain structure under an external field by grain boundary effects, such as the clamping of the domain walls and the hindrance of polarization switching, or the depolar-

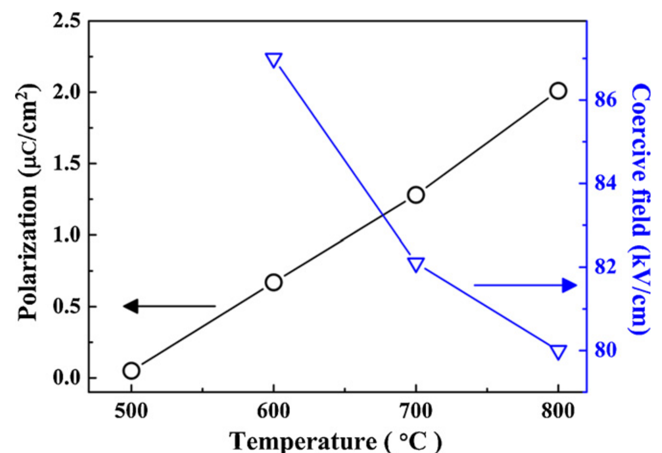

Fig. 6. Annealing temperature dependence of the remnant polarization and coercive field for the BTO films.

ization field originated by the low permittivity nonferroelectric grain boundaries.[30] Besides, the low crystallinity of 500 °C-annealed BTO is also a possible reason for the obtained low P_r. On the other hand, it should be noted that from XRD patterns for the BTO films, the separation of diffraction peaks (2 0 0) and (0 0 2) was not observed for all the annealed films. Meanwhile, the ferroelectricity is known to be attributed to the formation of tetragonal structure in materials. Thus, the different properties for the BTO thin films annealed at different temperatures suggests that a pseudocubic structure be formed in the BTO films having a larger grain size. The idea of the pseudocubic phase is based on a core–shell grain model in which individual grains consist of a cubic shell and a tetragonal grain interior.[32] Internal strains in tetragonal structure caused by the formation of nanoscale grains are believed to be responsible for its change to the so-called pseudocubic phase.[33,34] It can be considered that the obvious ferroelectricity observed in this work for the films after annealing at or above 600 °C is attributed to the formation of the pseudocubic phase, while the strong restrained ferroelectricity for the film annealed at 500 °C is due to the suppression of the tetragonal core caused by the smaller grain size.

To further study the change of the ferroelectricity with different grain size, Fig. 6 plots the remnant polarization (P_r) and coercive field (E_c) of the BTO films as a function of annealing temperatures. As the annealing temperature increases, the remnant polarization increases while the coercive field decreases. Since all the films have the same film thickness and the same in-plane tensile strain state, their grain size is then responsible solely for their different ferroelectric behaviors. Theoretical calculations have demonstrated that the density of 90° domain walls is inversely proportional to the square root of the grain size.[35] It means that the density of domain walls is increased with the decrease of annealing temperature, and consequently a distance dependent repulsive force between neighboring domain walls is enhanced. This leads to a reduction of the mobility for domain walls and more difficulty in domain orientation, resulting in the reduction of P_r and the increase of E_c.

4. Conclusions

In this work, ferroelectric BTO films were fabricated at room temperature by rf magnetron sputtering onto LNO buffered Si substrates. Post-annealings were then carried out at temperatures of 400–800 °C to obtained different grain size. It is found that the as-deposited BTO films are crystallized when the annealing temperature is higher than 500 °C and the crystallized BTO films exhibit a highly (1 0 0)-oriented texture. Ferroelectric measurement shows that although obvious ferroelectricity is observed for the films after annealing at temperatures ≥600 °C, however, a weak ferroelectricity is still obtained in 500 °C-annealed BTO. In combination with the XRD and TEM observations, it is suggested that a pseudocubic structure be formed in the BTO films when have large grain size around 20 nm. It has been also revealed that the P_r is reduced while E_c is increased for the BTO films as the grain size is decreased, which is discussed in terms of the change of density of domain walls in the films.

Acknowledgment

This work is supported by the Innovation Foundation of BUAA for Ph.D. Graduates and program for New Century Excellent Talents in university (NCET-04-0160) and Innovative Research Team in University(IRT0512).

References

1. Buscaglia, M. T., Viviani, M., Buscaglia, V., Mitoseriu, L., Testino, A., Nanni, P. *et al.*, High dielectric constant and frozen macroscopic polarization in dense nanocrystalline $BaTiO_3$ ceramics. *Phys. Rev. B*, 2006, **73**, 064114.
2. Canulescu, S., Dinescu, G., Epurescu, G., Matei, D. G., Grigoriu, C., Craciun, F. *et al.*, Properties of $BaTiO_3$ thin films deposited by radiofrequency beam discharge assisted pulsed laser deposition. *Mater. Sci. Eng. B*, 2004, **109**, 160.
3. Huang, L. M., Chen, Z. Y., Wilson, J. D., Banerjee, S., Robinson, R. D., Herman, I. P. *et al.*, Barium titanate nanocrystals and nanocrystal thin films: Synthesis, ferroelectricity, and dielectric properties. *J. Appl. Phys.*, 2006, **100**, 034316.
4. Ring, K. M. and Kavanagh, K. L., Substrate effects on the ferroelectric properties of fine-grained $BaTiO_3$ films. *J. Appl. Phys.*, 2003, **94**, 5982.
5. Han, H., Zhong, J., Kotru, S., Padmini, P., Song, X. Y. and Pandey, R. K., Improved ferroelectric property of $LaNiO_3$/$Pb(Zr_{0.2}Ti_{0.8})O_3$/$LaNiO_3$capacitors prepared by chemical solution deposition on platinized silicon. *Appl. Phys. Lett.*, 2006, **88**, 092902.
6. Yoon, K. H., Sohn, J.-H., Lee, B. D. and Kang, D. H., Effect of $LaNiO_3$ interlayer on dielectric properties of $(Ba_{0.5}Sr_{0.5})TiO_3$ thin films deposited on differently oriented Pt electrodes. *Appl. Phys. Lett.*, 2002, **81**, 5012.
7. Bao, D. H., Mizutani, N., Yao, X. and Zhang, L. Y., Structural, dielectric, and ferroelectric properties of compositionally graded (Pb, La)TiO_3 thin films with conductive $LaNiO_3$ bottom electrodes. *Appl. Phys. Lett.*, 2000, **77**, 1041.
8. Zou, Q., Ruda, H. E. and Yacobi, B. G., Improved dielectric properties of lead zirconate titanate thin films deposited on metal foils with $LaNiO_3$ buffer layers. *Appl. Phys. Lett.*, 2001, **78**, 1282.
9. Bao, D. H., Wakiya, N., Shinozaki, K., Mizutani, N. and Yao, X., Improved electrical properties of (Pb, La)TiO thin films using compositionally and structurally compatible $LaNiO_3$ thin films as bottom electrodes. *Appl. Phys. Lett.*, 2001, **78**, 3286.
10. Cheng, J. R., He, L., Yu, S. W. and Meng, Z. Y., Detection of residual stresses in $Pb(Zr_{0.53}Ti_{0.47})O_3$ thin films prepared on $LaNiO_3$ buffered metal substrates with Raman spectroscopy. *Appl. Phys. Lett.*, 2006, **88**, 152906.
11. Schlag, S. and Eicke, H. F., Size driven phase transition in nanocrystalline $BaTiO_3$. *Solid State Commun.*, 1994, **91**, 883.
12. Zhong, W., Jiang, B., Zhang, P., Ma, J., Chen, H., Yang, Z. *et al.*, Phase transition in $PbTiO_3$ ultrafine particles of different sizes. *J. Phys. Condens. Matter*, 1993, **5**, 2619.
13. Chattopanhuay, S., Ayyub, P., Palkar, V. R. and Multani, M., Size-induced diffuse phase transition in the nanocrystalline ferroelectric $PbTiO_3$. *Phys. Rev. B*, 1995, **52**, 13177.
14. Li, S., Eastman, J. A., Vetrone, J. M., Foster, C. M., Newnham, R. E. and Cross, L. E., Dimension and Size Effects in Ferroelectrics. *Jpn. J. Appl. Phys., Part I*, 1997, **36**, 5169.
15. Maruyama, T., Saitoh, M., Sakay, I. and Hidaka, T., Growth and characterization of 10-nm-thick c-axis oriented epitaxial $PbZr_{0.25}Ti_{0.75}O_3$ thin films on (1 0 0)Si substrate. *Appl. Phys. Lett.*, 1998, **73**, 3524.
16. Kim, Y. S., Kim, D. H., Kim, J. D., Chang, Y. J., Noh, T. W., Kong, J. H. *et al.*, Critical thickness of ultrathin ferroelectric $BaTiO_3$ films. *Appl. Phys. Lett.*, 2005, **86**, 102907.
17. Junquera, J. and Ghosez, P., Critical thickness for ferroelectricity in perovskite ultrathin films. *Nature*, 2003, **422**, 506.
18. Fong, D. D., Stephenson, G. B., Streiffer, S. K., Eastman, J. A., Auciello, O., Fuoss, P. H. *et al.*, Ferroelectricity in Ultrathin Perovskite Films. *Science*, 2004, **304**, 1650.

19. Qiao, L. and Bi, X. F., Dielectric response and structure of in-plane tensile strained $BaTiO_3$ thin films grown on the $LaNiO_3$ buffered Si substrate. *Appl. Phys. Lett.*, 2008, **92**, 062912.
20. Qiao, L. and Bi, X. F., Microstructure and ferroelectric properties of $BaTiO_3$ films on $LaNiO_3$ buffer layers by rf sputtering. *J. Cryst. Growth*, 2008, **310**, 2780.
21. Meier, A. R., Niu, F. and Wessels, B. W., Integration of $BaTiO_3$ on Si (0 0 1) using MgO/STO buffer layers by molecular beam epitaxy. *J. Cryst. Growth*, 2006, **294**, 401.
22. Dkhil, B., Defay, E. and Guillan, Strains in $BaTiO_3$ thin film deposited onto Pt-coated Si substrate. *J. Appl. Phys. Lett.*, 2007, **90**, 022908.
23. Huang, H., Yao, X., Wang, M. Q. and Wu, X. Q., $BaTiO_3$ on $LaNiO_3$ and Si thin films prepared by mist plasma evaporation. *J. Cryst. Growth*, 2004, **263**, 406.
24. Guo, Y. P., Suzuki, K., Nishizawa, K., Miki, T. and Kato, K., Dielectric and piezoelectric properties of highly (1 0 0)-oriented $BaTiO_3$ thin film grown on a Pt/TiOx/SiO_2/Si substrate using $LaNiO_3$ as a buffer layer. *J. Cryst. Growth*, 2005, **284**, 190.
25. Tang, L., Laughlin, D. E., Lambeth, D. N. and Doerner, M. F., Microstructure and magnetic properties of CoCrPt/Cr films on ultrasmooth NiP/AlMg substrates. *J. Appl. Phys.*, 1996, **79**, 5348.
26. Tang, L. and Thomas, G., Microstructure and texture evolution of Cr thin films with thickness. *J. Appl. Phys.*, 1993, **74**, 5025.
27. Thomas, R., Varadan, V. K., Komarneni, S. and Dube, D. C., Diffuse phase transitions, electrical conduction, and low temperature dielectric properties of sol-gel derived ferroelectric barium titanate thin films. *J. Appl. Phys.*, 2001, **90**, 1480.
28. Kim, Y. S., Jo, J. Y., Kim, D. J., Chang, Y. J., Lee, J. H., Noh, T. W. *et al.*, Ferroelectric properties of $SrRuO_3$/$BaTiO_3$/$SrRuO_3$ ultrathin film capacitors free from passive layers. *Appl. Phys. Lett.*, 2006, **88**, 072909.
29. Choi, K. J., Biegalski, M., Li, Y. L., Sharan, A., Schubert, J., Uecker, R. *et al.*, Enhancement of Ferroelectricity in Strained $BaTiO_3$ Thin Films. *Science*, 2004, **306**, 1005.
30. Deng, X. Y., Wang, X. H., Wen, H., Chen, L. L., Chen, L. and Li, L. T., Ferroelectric properties of nanocrystalline barium titanate ceramics. *Appl. Phys. Lett.*, 2006, **88**, 252905.
31. Wang, X. H., Deng, X. Y., Wen, H. and Li, L. T., Phase transition and high dielectric constant of bulk dense nanograin barium titanate ceramics. *Appl. Phys. Lett.*, 2006, **89**, 162902.
32. Liu, G., Wang, X. H., Lin, Y., Li, L. T. and Nan, C. W., Growth kinetics of core-shell-structured grains and dielectric constant in rare-earth-doped $BaTiO_3$ ceramics. *J. Appl. Phys.*, 2005, **98**, 044105.
33. Park, Y. and Kim, H.-G., Dielectric temperature characteristics of cerium-modified barium titanate based ceramics with core-shell grain structure. *J. Am. Ceram. Soc.*, 1997, **80**(1), 106.
34. Takeuchi, T., Tabuchi, M., kageyama, H. and Suyama, Y., Preparation of dense $BaTiO_3$ ceramics with submicrometer grains by spark plasma sintering. *J. Am. Ceram. Soc.*, 1999, **82**(4), 939.
35. Arlt, G., Hennings, D. and de With, G., Dielectric properties of fine-grained barium titanate ceramics. *J. Appl. Phys.*, 1985, **58**, 1619.